Effect of Internal Heat Generation on Free Convection Flow of Non-Newtonian Fluids over A Vertical Truncated Cone in Porous Media: VWT/VWC

飽和多孔性介質內具內部熱源效應對於非牛頓流體流經一垂直截尾圓錐體自然對流影響:可變壁溫度/可變壁濃度

Kuo-Ann Yih, Chuo-Jeng Huang 易國安、黃卓礽 Department of Aircraft Engineering, Air Force Institute of Technology 飛機工程系,空軍航空技術學院

Abstract

The effect of the internal heat generation on coupled heat and mass transfer by the free convection flow of a viscous non-Newtonian fluid over a vertical truncated cone embedded in a saturated-porous medium is numerically analyzed. The surface of the vertical truncated cone is maintained at variable wall temperature and variable wall concentration (VWT/VWC). The internal heat generation is of an exponential decaying form. The transformed nonsimilar governing equations are obtained with the coordinate transformation being performed, and then solved by Keller box method (KBM). Comparisons with previously published work are performed and excellent agreement is obtained. Numerical data for the dimensionless temperature profile, the dimensionless concentration profile, the local Nusselt number and the local Sherwood number are presented in graphical and tabular forms for the internal heat generation coefficient A^* , the power-law index of the non-Newtonian fluid n, the dimensionless streamwise coordinate ξ , the exponent of VWT/VWC λ , the buoyancy ratio N, and the Lewis number Le. The physical aspects of the problem are discussed in details.

Keywords: internal heat generation, free convection, non-Newtonian fluids, vertical truncated cone, porous media, VWT/VWC

摘 要

本文以一數值方法分析:飽和多孔性介質內具內部熱源效應對於非牛頓流體流經一垂直截尾圓錐體之自然對流熱傳與質傳影響。垂直截尾圓錐體的表面維持於可變壁溫度/可變壁濃度條件。內部熱源的形式假設為指數漸減形式。吾人先執行座標轉換可得轉換後的非相似控制方程式,再以凱勒盒子法求解之。所得的數值計算結果首先與早期已刊登發表的論文結果作比較,結果非常吻合。本文數值計算的結果主要以圖形與表格的形式來顯示:內部熱源係數 A^* ,非牛頓流體之冪次律指標 n,無因次流線方向座標 ξ ,可變壁溫度/可變壁濃度指數 λ ,浮力比 N,路易士數 Le 對無因次溫度分佈、無因次濃度分佈、局部 Nusselt 數和局部

Sherwood 數之影響。文中的物理現象也詳加討論。

關鍵字: 內部熱源,自然對流,非牛頓流體,垂直截尾圓錐體,多孔性介質,可變壁溫度/可 變壁濃度

1. Introduction

The convective heat and mass transfer in a saturated porous medium has a number of important applications in geothermal and geophysical engineering. These include nuclear reactor cooling system, extraction of geothermal energy, thermal insulation of buildings, filtration processes and disposal of underground nuclear wastes. Recent books by Nield and Bejan [1], Ingham and Pop [2] and Vafai [3] present a comprehensive account of the available information in the field.

A number of industrially important fluids, including fossil fuels which can saturate underground beds, display the behavior of non-Newtonian. The non-linear relationship between shear strain rate and shear stress of non-Newtonian fluids in porous matrix is quite different from that of Newtonian fluids in porous media. In the aspect of pure heat transfer, Chen and Chen [4], Wang and Tu [5] and Gorla and Kumari [6] investigated the case of the vertical flat plate, respectively. Nakayama and Koyama [7], Hossain and Nakayama [8], Yang and Wang [9], and Wang et al. [10] examined individually the body of arbitrary shape. The case of the vertical cone was considered by Yih [11], Cheng [12], and Mahmoud [13], respectively.

In the aspect of coupled heat and mass transfer, double-diffusion from a vertical surface in a porous region saturated with a non-Newtonian fluid was studied by Rastogi and Poulikakos [14]. Cheng [15-16] examined the natural convection heat and mass transfer of non-Newtonian power law fluids in

porous media from a vertical truncated cone with variable wall temperature and concentration [15], and variable heat and mass fluxes [16], respectively.

The effect of the internal heat generation is important in several applications that include reactor safety analyses, metal waste form development for spent nuclear fuel, fire and combustion studies, and the storage of radioactive materials. A new class of similarity solutions has obtained for isothermal vertical plate in a semi-infinite quiescent fluid with internal heat generation decaying exponentially by Crepeau and Clarksean [17]. Postelnicu and Pop [18] studied the similarity solutions of free convection boundary layers over vertical and horizontal surfaces in porous media with internal heat generation. Postelnicu et al. [19] presented the case of the vertical permeable flat plate. Bagai [20] analyzed similarity solutions of free convection boundary layers over a body of arbitrary shape in a porous medium with internal heat generation. Effect of variable viscosity on free convection over a nonisothermal axisymmetric body in a porous medium with internal heat generation investigated by Bagai [21]. Mohamed [22] performed the similarity solution for the effect of lateral mass flux on the natural convection boundary layers induced by a heated vertical plate embedded in a saturated porous medium with internal heat generation.

Grosan and Pop [23] extended the research of Chen and Chen [4] to examine the free convection over vertical flat plate with a variable wall temperature and internal heat generation in a porous medium saturated with a non-Newtonian fluid. Grosan et al. [24] studied the free convection boundary layer over a vertical cone in a non-Newtonian fluid saturated porous medium with internal heat generation. Bagai and Nishad [25] investigated the free convection in a non-Newtonian fluid along a horizontal plate embedded in porous media with internal heat generation. Recently, Yih and Huang [26] extended the work of Grosan and Pop [23] to examine the effect of internal heat generation on free convection heat and mass transfer of non-Newtonian fluids flow over a vertical plate in porous media: VWT/VWC.

Therefore, the objective of the present work is to extend the work of Cheng [15], Grosan and Pop [23], Grosan et al. [24], and Yih and Huang [26] to investigate the internal heat generation effect on the couple heat and mass transfer by the free convection flow of a viscous non-Newtonian fluid over a vertical truncated cone embedded in a saturated porous medium: VWT/VWC. It is assumed that the internal heat generation is of the exponential decaying form. The governing equations have been solved numerically using Keller box method (KBM). The results are obtained and discussed for various values of the parameters.

2. Analysis

Let us consider the problem of the influence of the internal heat generation on combined heat and mass free convection flow of a viscous non-Newtonian fluid over a vertical truncated cone (with half angle γ) embedded in a fluid-saturated porous medium. Figure 1 shows the flow model and the physical coordinate system. The origin of the coordinate system is placed at the vertex of the full

cone, where x is the coordinate along the surface of cone measured from the origin and y is the coordinate normal to the surface, respectively. We consider the boundary condition of variable wall temperature $T_{\rm w}$ and variable wall concentration $C_{\rm w}$ (VWT/VWC); $T_{\rm w}$ and $C_{\rm w}$ are higher than the ambient temperature T_{∞} and ambient concentration C_{∞} , respectively. The variations of fluid properties are limited to density variation that affects the buoyancy force term only. The viscous dissipation effect is neglected for the low velocity.

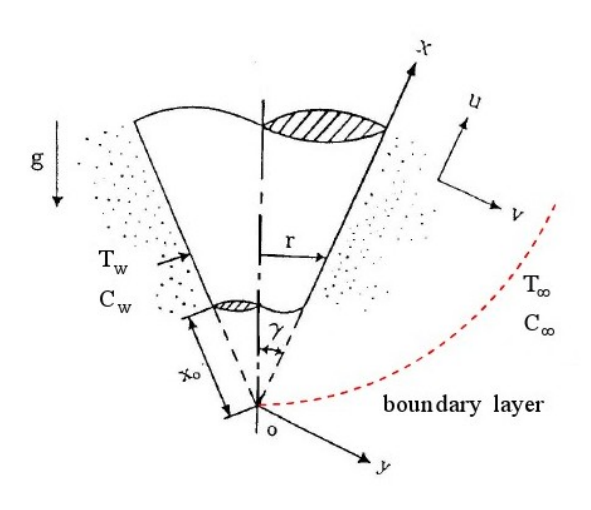


Fig. 1. The flow model and the physical coordinate system

Introducing the boundary layer and Boussinesq approximations, the governing equations and the boundary conditions based on the Darcy law (It is valid under the condition of low velocity and small pores of porous medium [27]) can be written as follows:

Continuity equation:

$$\frac{\partial (ru)}{\partial x} + \frac{\partial (rv)}{\partial y} = 0, \tag{1}$$

Momentum (Darcy) equation:

$$u^{n} = -\frac{K(n)}{\mu} \left(\frac{\partial p}{\partial x} + \rho g \cos \gamma \right), \tag{2}$$

$$v^{n} = -\frac{K(n)}{\mu} \left(\frac{\partial p}{\partial y} + \rho g \sin \gamma \right), \tag{3}$$

Energy equation:

$$u\frac{\partial T}{\partial x} + v\frac{\partial T}{\partial y} = \alpha \frac{\partial^2 T}{\partial y^2} + \frac{q'''}{\rho_{\infty} C_p},$$
 (4)

Concentration equation:

$$u\frac{\partial C}{\partial x} + v\frac{\partial C}{\partial v} = D_M \frac{\partial^2 C}{\partial v^2},$$
 (5)

Boussinesq approximation:

$$\rho = \rho_{\infty} \big[1 - \beta_{T} \big(T - T_{\infty} \big) - \beta_{C} \big(C - C_{\infty} \big) \big], \qquad (6)$$

Boundary conditions:

$$y = 0$$
: $v = 0$, $T = T_{\infty} + a(x - x_{0})^{\lambda}$,
 $C = C_{\infty} + b(x - x_{0})^{\lambda}$, (7.1-3)

$$y \to \infty$$
: $u = 0$, $T = T_{\infty}$, $C = C_{\infty}$. (8.1-3)

Here, r is the local radius of the vertical truncated cone; u and v are the Darcian velocities in the x- and y- directions; K(n) is the modified permeability of the porous medium; n is the power-law index of the non-Newtonian fluid; g is the gravitational acceleration; μ , p and ρ are the modified viscosity, the pressure and the density of the fluid, respectively; T and C are the volume-averaged temperature and concentration, respectively; α and $D_{\scriptscriptstyle M}$ are the equivalent thermal diffusivity and mass diffusivity, respectively; q" is the internal heat generation rate per unit volume; C_p is the specific heat at constant pressure; β_T and β_C are the thermal and concentration expansion coefficients of the fluid, respectively; a and b are positive constants; λ is the exponent of VWT/VWC.

We assumed the boundary layer to be sufficiently thin in comparison with the local radius of the vertical truncated cone. The local radius to a point in the boundary layer, therefore, can be

replaced by the radius of the vertical truncated cone, i.e., $r = x \sin \gamma$. Equations (1)-(8) are valid in $x_o \le x < \infty$ where x_o is the distance of the leading edge of the vertical truncated cone measured from the origin.

The power law fluid index n for various fluids is as follows:

- (i) n < 1 for pseudo-plastic fluids (for example, the polymer solution) or shear-thinning fluids that have a lower apparent viscosity at higher shear rates.
- (ii) n = 1 for Newtonian fluids (for instance, air and water) where the shear stress is directly proportional to the shear rate.
- (iii) n > 1 for dilatant fluids (for example, the suspensions of sand) or shear-thickening fluids for which there is an increase in the apparent viscosity at higher shear rates.

For the power law model of Ostwald-de-Waele, Christopher and Middleman [28] and Dharmadhikari and Kale [29] proposed the following relationships for the permeability:

$$K(n) = \begin{cases} \frac{6}{25} \left(\frac{n\varepsilon}{3n+1}\right)^n \left[\frac{\varepsilon d}{3(1-\varepsilon)}\right]^{n+1} & [28] \\ \frac{2}{\varepsilon} \left[\frac{d\varepsilon^2}{8(1-\varepsilon)}\right]^{n+1} \left(\frac{6n+1}{10n-3}\right) \left(\frac{16}{75}\right)^{\frac{3(10n-3)}{(10n+11)}} & [29] \end{cases}$$

(9)

where d is the particle diameter while ϵ is the porosity.

The stream function ψ is defined by

$$ru = \partial \psi / \partial y$$
, $rv = -\partial \psi / \partial x$. (10)

Therefore, the continuity equation is automatically satisfied.

We now pay attention to the governing equations (2) and (3). If we do the cross-differentiation $\partial(u^n)/\partial y - \partial(v^n)/\partial x$, then the

pressure terms in equations (2) and (3) can be eliminated. Further, with the help of the equation (6) and the boundary layer approximation $(\partial/\partial x << \partial/\partial y)$, and assuming that g cos γ and g sin γ are of the same order of magnitude, then we can obtain

$$\frac{\partial u^{n}}{\partial y} = \frac{\rho_{\infty} g \cos \gamma K(n)}{\mu} \left(\beta_{T} \frac{\partial T}{\partial y} + \beta_{C} \frac{\partial C}{\partial y} \right). \quad (11)$$

Integrating equation (11) once and with the aid of boundary condition (8.1-3), then we get

$$u^{n} = \frac{\rho_{\infty}g\cos\gamma K(n)}{\mu} \left[\beta_{T}(T - T_{\infty}) + \beta_{C}(C - C_{\infty})\right]$$

(12)

Invoking the following dimensionless non-similarity variables:

$$\xi = \frac{x^*}{x_0} = \frac{x - x_0}{x_0} \tag{13.1}$$

$$\eta = \frac{y}{x^*} Ra_{x^*}^{\frac{1}{2}n}$$
 (13.2)

$$f(\xi, \eta) = \frac{\Psi}{\alpha \operatorname{rRa}^{\frac{1}{2}n}}$$
 (13.3)

$$\theta(\xi, \eta) = \frac{T - T_{\infty}}{T_{w} - T_{\infty}}$$
 (13.4)

$$\phi(\xi, \eta) = \frac{C - C_{\infty}}{C_{w} - C_{\infty}}$$
 (13.5)

$$Ra_{x^*} = \frac{\rho_{\infty}g\cos\gamma\beta_{T} \left[T_{w} - T_{\infty}\right] K(n)}{\mu} \left(\frac{x^*}{\alpha}\right)^{n}$$

(13.6)

The internal heat generation rate per unit volume q" is modeled according to the following equation [18-26]:

$$q''' = A^* \frac{k Ra_{x^*}^{\frac{1}{N}}}{\left(x^*\right)^2} \left[T_w - T_{\infty}\right] e^{-\eta}.$$
 (14)

Here, k is the equivalent thermal conductivity. A* is the internal heat generation coefficient. Note that

when $A^* = 0$ corresponds to the case 1: no internal heat generation (designated as NIHG); while for $A^* > 0$ corresponds to the case 2: with internal heat generation (WIHG).

Substituting equations (13)-(14) into equations (12), (4)-(5), (7)-(8), we obtain

$$(f')^n = \theta + N \phi, \tag{15}$$

$$\theta'' + \left(\frac{\xi}{1+\xi} + \frac{n+\lambda}{2n}\right) f \theta' - \lambda f'\theta + A^* e^{-\eta}$$

$$= \xi \left(f' \frac{\partial \theta}{\partial \xi} - \theta' \frac{\partial f}{\partial \xi}\right), \tag{16}$$

$$\frac{1}{Le} \phi'' + \left(\frac{\xi}{1+\xi} + \frac{n+\lambda}{2n}\right) f \phi' - \lambda f' \phi$$

$$= \xi \left(f' \frac{\partial \phi}{\partial \xi} - \phi' \frac{\partial f}{\partial \xi}\right). \tag{17}$$

The boundary conditions are defined as follows:

$$\eta = 0$$
: $f = 0$, $\theta = 1$, $\phi = 1$, (18)

$$\eta \to \infty$$
: $\theta = 0, \ \phi = 0.$ (19)

In addition, in terms of the new variables, the Darcian velocities in x- and y- directions are, respectively, given by

$$u = \frac{\alpha R a_{x}^{\frac{\gamma_{n}}{n}}}{x^{*}} f', \qquad (20)$$

$$v = -\frac{\alpha R a_{x^*}^{\frac{1}{2}n}}{x^*} \left[\left(\frac{\xi}{1+\xi} + \frac{n+\lambda}{2n} \right) f + \xi \frac{\partial f}{\partial \xi} - \left(\frac{n-\lambda}{2n} \right) \eta f' \right]. \tag{21}$$

where primes denote differentiation with respect to η . Ra_x is the modified local Rayleigh number for the flow through the porous medium

Besides, the buoyancy ratio N and the Lewis number Le are defined as followed, respectively:

$$N = \frac{\beta_{\rm C} \left[C_{\rm w} - C_{\infty} \right]}{\beta_{\rm T} \left[T_{\rm w} - T_{\infty} \right]} = \frac{\beta_{\rm C} b}{\beta_{\rm T} a}, \qquad \text{Le} = \frac{\alpha}{D_{\rm M}}. \quad (22)$$

The results of practical interest in many applications are both the surface heat and mass

transfer rates. The surface heat and mass transfer rates are expressed in terms of the local Nusselt number $\mathrm{Nu}_{\mathrm{x}^*}$ and the local Sherwood number $\mathrm{Sh}_{\mathrm{x}^*}$ respectively, which are basically defined as followed:

$$Nu_{x^*} = \frac{h_{x^*} x^*}{k} = \frac{q_w x^*}{[T_w - T_{\infty}] k}.$$
 (23)

$$Sh_{x^*} = \frac{h_{m,x^*} x^*}{D_M} = \frac{m_w x^*}{[C_w - C_\infty] D_M}.$$
 (24)

where h_{x^*} , h_{m,x^*} are local convective heat transfer coefficient and local convective mass transfer coefficient, respectively; q_w and m_w are the local heat flux and the local mass flux, respectively; and $q_w = h_{x^*} \big[T_w - T_\infty \big]$ (the Newton's law of cooling) and $m_w = h_{m,x^*} \big[C_w - C_\infty \big]$ (the analogy between the mass transfer and the heat transfer).

From the Fourier's law of heat conduction and the Fick's law of mass diffusion, the rate of surface heat transfer $q_{\rm w}$ and the rate of surface mass transfer $m_{\rm w}$ are defined as followed, respectively:

$$q_{w} = -k \left(\frac{\partial T}{\partial y} \right)_{v=0}.$$
 (25)

$$m_{\rm w} = -D_{\rm M} \left(\frac{\partial C}{\partial y} \right)_{y=0}$$
 (26)

Inserting equations (25)-(26) into equations (23)-(24) and with the aid of equation (13), the local Nusselt number Nu_{x} and the local Sherwood number Sh_{x} in terms of $Ra_{x}^{\frac{1}{2}n}$ are, respectively, obtained by

$$\frac{Nu_{x^*}}{Ra_{x^*}^{1/2}} = -\theta'(\xi, 0). \tag{27}$$

$$\frac{Sh_{x^*}}{Ra_{x^*}^{1/2}} = -\phi'(\xi, 0). \tag{28}$$

On the one hand, for the case of N = 0 (pure heat transfer), $\xi = \gamma = 0$ (vertical flat plate), and $A^* = 1$ (WIHG), equations (15)-(16), (18.1-2)-(19.1) are reduced to those of Grosan and Pop [23] where a similar solution was obtained previously. (The boundary value problem for \$\phi\$ then becomes ill-posed and is of no physical significance). On the other hand, for N = 0 and $\xi \rightarrow \infty$ (vertical cone), and $A^* = 1$, equations (15)-(16), (18.1-2)-(19.1) are reduced to those of Grosan et al. [24] where a similar solution was obtained previously. It may be also noticed that for the case of $A^* = 0$ (NIHG), equations (15)-(19) are reduced to those of Cheng [15] where a nonsimilar solution was obtained previously. For the case of $\xi = \gamma = 0$, equations (15)-(19) are reduced to those of Yih and Huang [26] where a similar solution was obtained previously.

3. Numerical Method

The present analysis integrates the system of equations (15)-(19) by the implicit finite difference approximation together with the modified Keller box method of Cebeci and Bradshaw [30]. To begin with, the partial differential equations are first converted into a system of five first-order equations. Then these first-order equations are expressed in finite difference forms and solved along with their boundary conditions by an iterative scheme. This approach gives a better rate of convergence and reduces the numerical computational times.

Computations were carried out on a personal computer with the first step size $\Delta \eta_1 = 0.01$. The

variable grid parameter is chosen 1.01 and the value of $\eta_{\infty}=10$. The iterative procedure is stopped to give the final temperature and concentration distributions when the errors in computing the $|\theta'_{\rm w}|$ and $|\phi'_{\rm w}|$ in the next procedure become less than 10^{-5} .

4. Results and Discussion

In order to verify the accuracy of our present method, we have compared our results with those of Cheng [15], Grosan and Pop [23], Grosan et al. [24]. Table 1 shows the comparison of the values of $-\theta'(\xi,0)$ for various values of λ with N = 0 (pure heat transfer), $A^* = 0$ (NIHG), n = 1 (Newtonian fluid). Table 2 illustrates the comparison of the values of $-\theta'(0,0)$ for various values of n and λ with A^* = 0, N = 0, γ = 0 (vertical flat plate). Table 3 lists the comparison of the values of $-\theta'(0,0)$ for various values of n and λ with $A^* = 1$ (WIHG), N = 0, γ = 0. Table 4 shows the comparison of the values of $-\theta'(\infty,0)$ for various values of n and λ with A^* = 0, N = 0, (vertical full cone). Table 5 illustrates the comparison of the values of $-\theta'(\infty,0)$ for various values of n and λ with $A^* = 1$, N = 0. The comparisons in all the above cases are found to be in excellent agreement, as shown in Tables 1-5.

Table 1 Comparison of the values of $-\theta'(\xi,0)$ for various values of λ with $N=0 \text{ (pure heat transfer)}, \quad A^* = 0 \text{ (NIHG)},$

n = 1 (Newtonian fluid)

ξ	Chen	g [15]	Present results	
ک	$\lambda = 0$	$\lambda = 1/2$	$\lambda = 0$	$\lambda = 1/2$
0	0.4439	0.7704	0.4439	0.7704
1	0.5807	0.8675	0.5808	0.8676
10	0.7326	0.9659	0.7330	0.9661
∞	0.7686	0.9896	0.7685	0.9896

Here, $\xi \to \infty$ denotes $\xi = 10^4$.

Table 2 Comparison of the values of $-\theta'(0,0)$ for various values of n and λ with $A^* = 0$, N = 0, $\gamma = 0$ (vertical flat plate)

	Grosan ar	nd Pop [23]	Present results	
n	$\lambda = 0$	$\lambda = 1$	$\lambda = 0$	$\lambda = 1$
0.5	0.3777	0.9287	0.3778	0.9292
0.8	0.4240	0.9785	0.4241	0.9786
1.0	0.4439	0.9997	0.4439	1.0000
1.5	0.4754	1.0340	0.4754	1.0339
2.0	0.4938	1.0538	0.4938	1.0537
2.5	0.5059	1.0672	0.5058	1.0667

Table 3 Comparison of the values of $-\theta'(0,0)$ for various values of n and λ with $A^* = 1$ (WIHG), N $= 0, \quad \gamma = 0$

	Grosan and	Pop [23]	Present results	
n	$\lambda = 0$	$\lambda = 1$	$\lambda = 0$	$\lambda = 1$
0.5	-0.2754	0.4697	- 0.2756	0.4698
0.8	-0.2288	0.5084	-0.2290	0.5071
1.0	-0.2152	0.5254	- 0.2153	0.5241
1.5	-0.1921	0.5531	- 0.1923	0.5519
2.0	-0.1778	0.5699	-0.1780	0.5686
2.5	-0.1680	0.5811	-0.1684	0.5797

Table 4 Comparison of the values of $-\theta'(\infty,0)$ for various values of n and λ with

 $A^* = 0$, N = 0, (vertical full cone)

	n	Grosan e	et al. [24]	Present results	
		$\lambda = 0$	$\lambda = 1/2$	$\lambda = 0$	$\lambda = 1/2$
	0.5	0.6527	0.8828	0.6522	0.8825
	0.8	0.7340	0.9574	0.7338	0.9573
	1.0	0.7686	0.9897	0.7685	0.9896
	1.5	0.8233	1.0409	0.8233	1.0408
	2.0	0.8552	1.0710	0.8552	1.0709
	2.5	0.8762	1.0908	0.8760	1.0907

Table 5 Comparison of the values of $-\theta'(\infty,0)$ for various values of n and λ with

$$A^* = 1, N = 0$$

	Grosan	et al. [24]	Present results	
n	$\lambda = 0$	$\lambda = 1/2$	$\lambda = 0$	$\lambda = 1/2$
0.5	0.0939	0.3881	0.0932	0.3875

0.8	0.1646	0.4513	0.1641	0.4509
1.0	0.1962	0.4799	0.1957	0.4796
1.5	0.2477	0.5271	0.2473	0.5269
2.0	0.2787	0.5558	0.2783	0.5556
2.5	0.2994	0.5749	0.2991	0.5748

The numerical results are presented for the internal heat generation coefficient A^* ranging from 0 to 1, the power-law index of the non-Newtonian fluid n ranging from 0.5 to 2.0, the exponent of VWT/VWC λ ranging from 0 to 1, the dimensionless streamwise coordinate ξ ranging from 0 to 10^4 (designated as ∞), the buoyancy ratio N ranging from -0.5 to -0.5; the Lewis number Le ranging from 1 to 10.

The effects of the dimensionless streamwise coordinate & and the internal heat generation coefficient A* on the dimensionless temperature and concentration profiles with N = 1, Le = 5, n = 1.5, $\lambda = 0.5$ are illustrated in Figs. 2 and 3, respectively. In Fig. 2, for a given ξ , it is observed that the dimensionless temperature profile θ enhances with increasing the internal heat generation coefficient A*, thus thickening the thermal boundary layer thickness δ_T and decreasing the dimensionless wall temperature gradient $[-\theta'(\xi,0)]$. Moreover, for a given A*, the thermal boundary layer thickness becomes thin while the dimensionless wall temperature gradient raises with increasing the dimensionless streamwise coordinate ξ from ξ = $\gamma = 0$ (vertical flat plate) to $\xi = 10^4$ (vertical full cone).

Figure 3 shows that for a given ξ , the dimensionless concentration profile ϕ decreases with increasing the internal heat generation coefficient A^* , thus thinning the concentration boundary layer thickness δ_C and enhancing the dimensionless wall concentration gradient $\left[-\phi'(\xi,0)\right]$.

In addition, it is also found that under a given A^* , the concentration boundary layer thickness becomes thin, like the thermal boundary layer thickness (Fig. 2), but the dimensionless wall concentration gradient raises, like the dimensionless wall temperature gradient (Fig. 2), with increasing the dimensionless streamwise coordinate ξ from $\xi = \gamma = 0$ to $\xi = 10^4$.

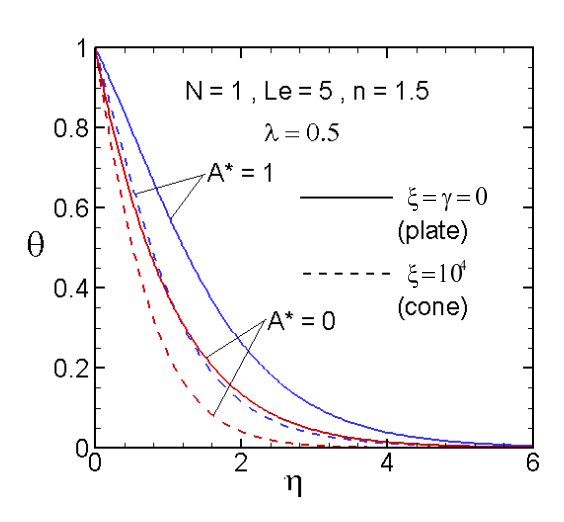


Fig. 2. The dimensionless temperature profile for two values of A^* and ξ

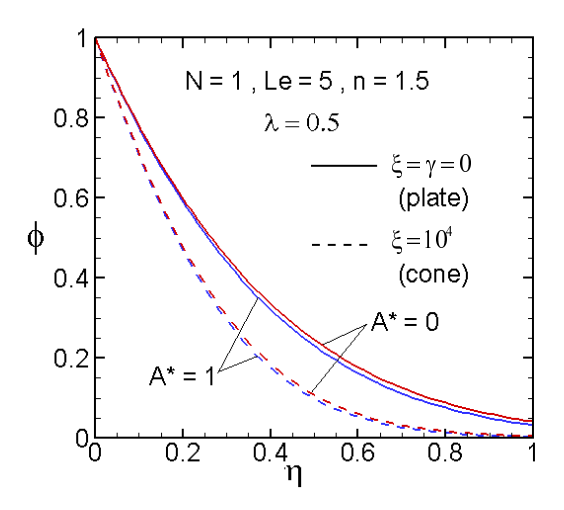


Fig. 3. The dimensionless concentration profile for two values of A^* and ξ

Figures 4 and 5 portray the dimensionless profile and the dimensionless temperature concentration profile for the two values of the buoyancy ratio N (N = -0.5, 5) and the Lewis number Le (Le = 1, 10) with $A^* = 1$, n = 0.5, $\xi =$ 1, $\lambda = 0$, respectively. In Fig. 4, for a fixed value of Le, as the buoyancy ratio N increases from -0.5 to 5, the thermal boundary layer thickness decreases yet the dimensionless wall temperature gradient enhances. Furthermore, it is also observed that for a positive buoyancy ratio N (N = 5), as the Lewis number Le increases from 1 to 10, the thermal boundary layer thickness becomes thick; however the dimensionless wall temperature gradient decreases. On the contrary, for a negative buoyancy ratio N (N = -0.5), the thermal boundary layer thickness becomes thin yet the dimensionless wall temperature gradient enhances. From Fig. 4, we can find that the dimensionless temperature profiles have the phenomena of overshoot for the case of N = -0.5 where the heat transfer is from the porous medium to the vertical truncated cone, as shown in Fig. 4. These interesting phenomena of overshoot are also found in the research of [18-26].

In Fig. 5, it is found that the dimensionless concentration profiles decrease monotonically from the surface to the ambient. On the one hand, for the fixed value of Le, the concentration boundary layer thickness, like the thermal boundary layer thickness (Fig. 4), becomes thin as the buoyancy ratio N increases. On the other hand, it is also seen that for the fixed value of N, when the Lewis number Le increases from 1 to 10, the concentration boundary layer thickness becomes thin.

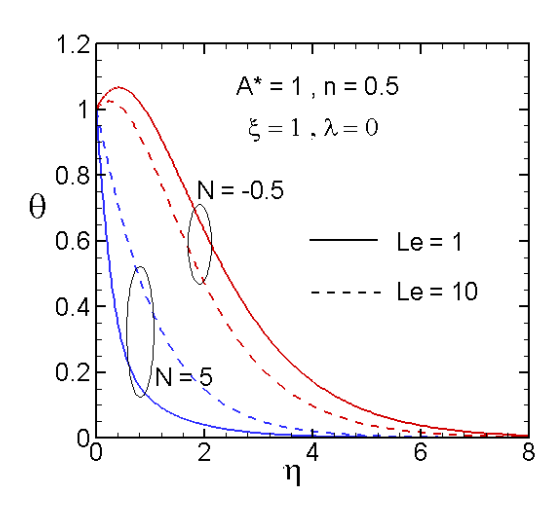


Fig. 4. The dimensionless temperature profile for two values of N and Le

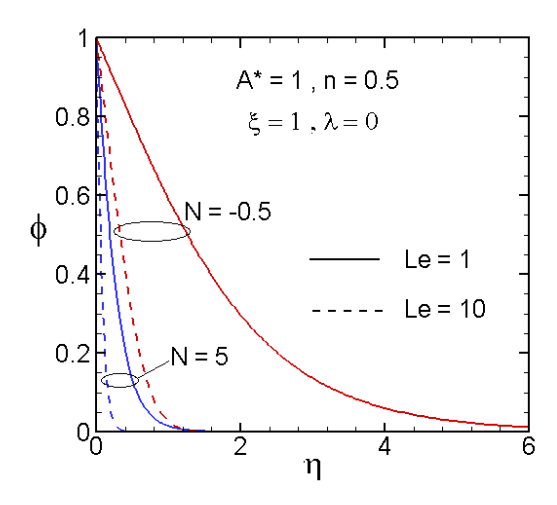


Fig. 5. The dimensionless concentration profile for two values of N and Le

The effect of power-law index n and the exponent of VWT/VWC λ on the dimensionless temperature profile and the dimensionless concentration profile with N = 2, Le = 3, A* = 1, ξ = 10 are plotted in Figs. 6 and 7, respectively. In these two figures, for a fixed n, it is observed that both the dimensionless temperature profile and the dimensionless concentration profile decrease with increasing the exponent of VWT/VWC λ , thus

increasing both the dimensionless wall temperature gradient and the dimensionless wall concentration gradient.

In Fig. 6, for a fixed λ , the non-Newtonian fluid with lower power-law index n (n = 0.5) has the greater dimensionless wall temperature gradient. Besides, Fig. 7 shows that the non-Newtonian fluid with lower power-law index n (n = 0.5) has the thinner concentration boundary layer thickness as well as the greater dimensionless wall concentration gradient.

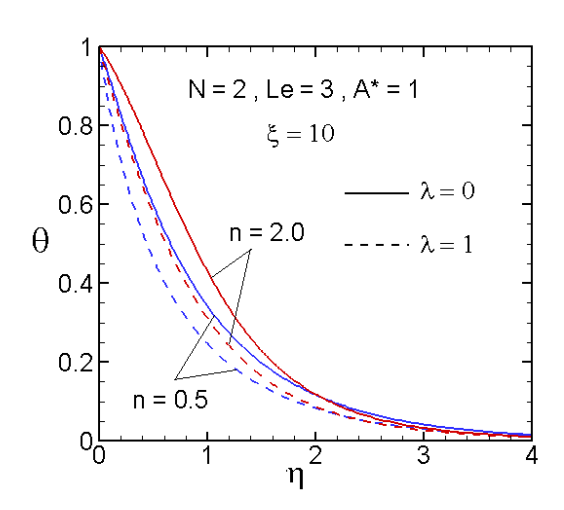


Fig. 6. The dimensionless temperature profile for two values of n and λ

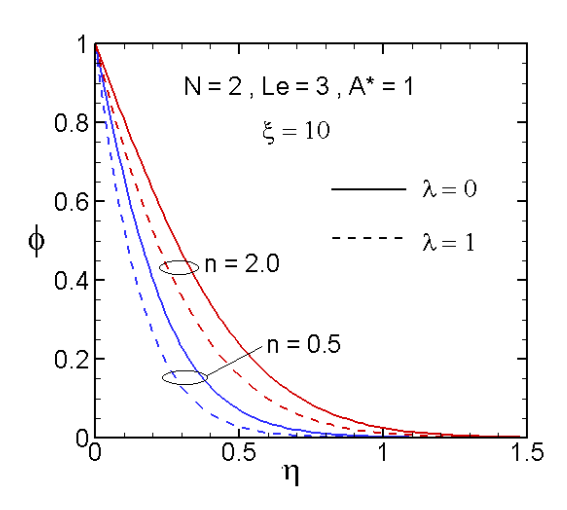


Fig. 7. The dimensionless concentration profile for two values of n and λ

Figures 8 and 9 illustrate the variation of the local Nusselt number $Nu_x/Ra_x^{\frac{1}{2}n}$ and the local Sherwood number $Sh_x/Ra_x^{\frac{1}{2}n}$ for the dimensionless streamwise coordinate ξ with various values of the internal heat generation coefficient A^* (A^* ranging from 0 to 1) with N=1, Le = 5, n=1.5, $\lambda=0.5$, respectively. In Fig. 8, for the fixed ξ , the local Nusselt number tends to decrease as the internal heat generation coefficient A^* is increased. This is because increasing the internal heat generation coefficient A^* increases the thermal boundary layer thickness, as shown in Fig. 2. The thicker the thermal boundary layer thickness, the smaller the local Nusselt number.

Figure 9 shows that, for fixed ξ , the local Sherwood number tends to slightly increase as the internal heat generation coefficient A^* is increased. This is because increasing the internal heat generation coefficient A^* decreases the concentration boundary layer thickness, as shown in Fig. 3. The thinner the concentration boundary layer thickness, the greater the local Sherwood number.

In both Figs. 8 and 9, it is also shown that, for the fixed A^* , increasing the value of the dimensionless streamwise coordinate ξ enhances the local Nusselt number as well as the local Sherwood number. This is because the increase in the value of ξ decreases both the thermal boundary layer thickness and the concentration boundary layer thickness, as shown in Figs. 2 and 3. The thinner the thermal (concentration) boundary layer thickness, the larger the local Nusselt (Sherwood) number. It is also observed that not only the local Nusselt number but also the local Sherwood number approaches to constant value when ξ is small ($\xi = 10^{-3}$: vertical flat plate) and large ($\xi = 10^4$: vertical full cone).

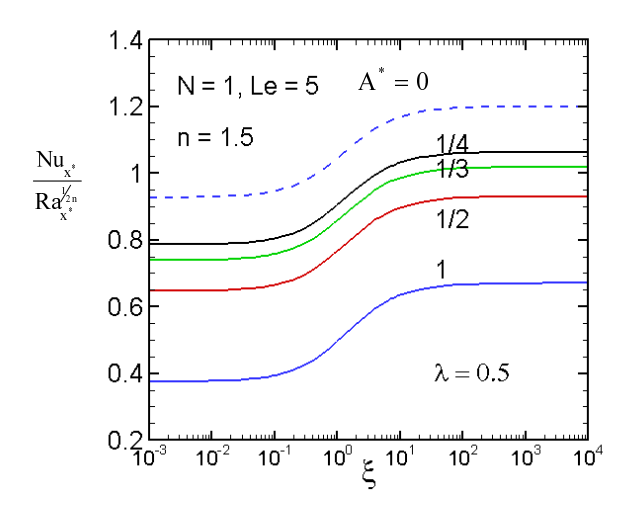


Fig. 8. Effect of A* on the local Nusselt number

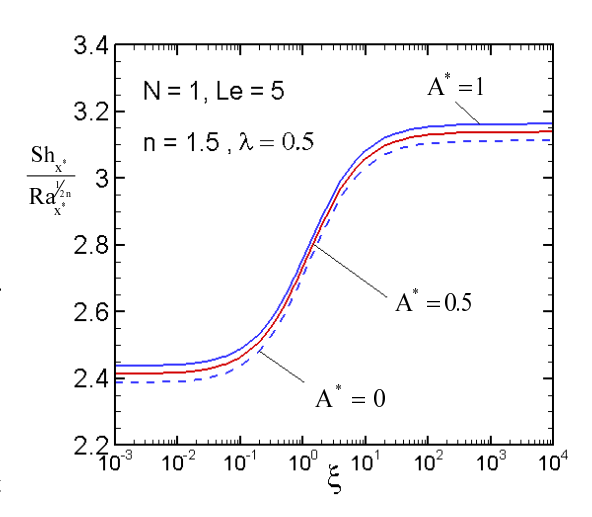


Fig. 9. Effect of A* on the local Sherwood number

Figures 10 and 11 portray the local Nusselt $Nu_{x^*}/Ra_{x^*}^{1/2}$ and the local Sherwood number $\operatorname{Sh}_{\mathbf{x}^*}/\operatorname{Ra}_{\mathbf{x}^*}^{\frac{1}{2}n}$ number functions the dimensionless streamwise coordinate ξ for the two values of the buoyancy ratio N (N = -0.5, 5) and the Lewis number Le (Le = 1, 10) with $A^* = 1$, n =0.5, $\lambda = 0$, respectively. In Fig. 10, for a fixed value of Le, it is observed that the local Nusselt number increases with increasing the buoyancy ratio N. This is because the increase in the value of N tends to increase the buoyancy force, accelerating the flow and thereby the thermal boundary layer thickness becomes thin, as shown in Fig. 4. For a given positive N (N = 5), as the Lewis number increases from 1 to 10, the local Nusselt number decreases. This is due to the fact that a larger Lewis number Le is associated with a thicker thermal boundary layer thickness. The thicker the thermal boundary layer thickness, the smaller the local Nusselt number. Whereas, for a given negative N (N = -0.5), as the Lewis number is increased from 1 to 10, the local Nusselt number increases, as revealed in Fig. 10.

In Fig. 11, it is observed that the local Sherwood number also, like the local Nusselt number (Fig. 10), enhances as the buoyancy ratio N increases for a fixed value of Le. This is also because the increase in the value of N reduces the concentration boundary layer thickness, as shown in Fig. 5. For a given N, as the Lewis number Le increases from 1 to 10, the local Sherwood number also increases. This is because that a larger Lewis number Le is associated with a thinner concentration boundary layer thickness. The thinner the concentration boundary layer thickness, the greater the local Sherwood number. The Lewis number Le has a more significant effect on the local Sherwood number than it does on the local Nusselt number, as compared Figs. 10 and 11.

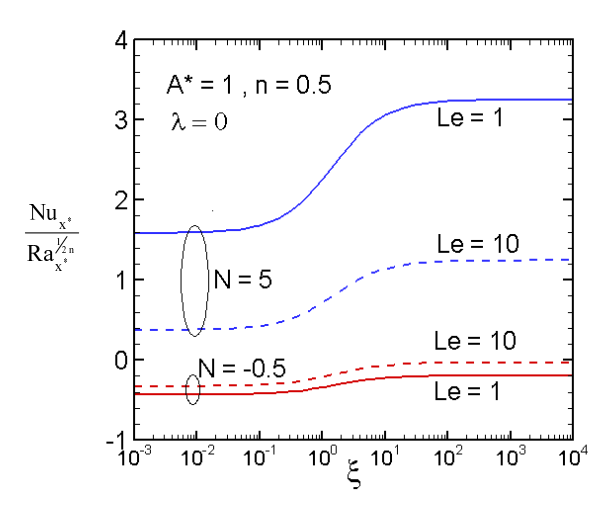


Fig. 10. Effect of N and Le on the local Nusselt number

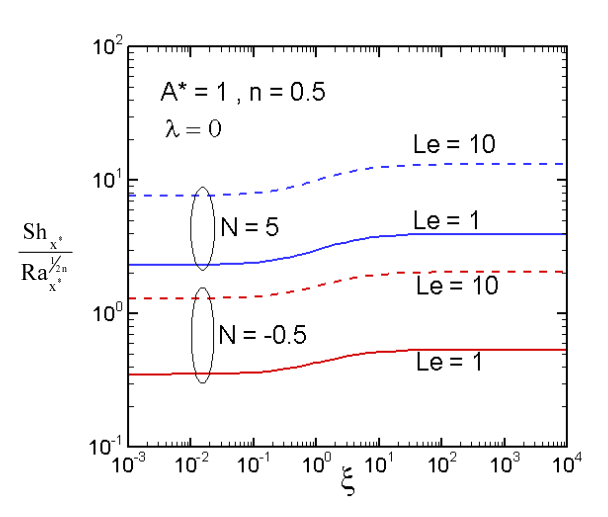


Fig. 11. Effect of N and Le on the local Sherwood number

Figures 12 and 13 plot the local Nusselt number $Nu_{\mathbf{v}^*} / Ra_{\mathbf{x}^*}^{\frac{1}{2}n}$ and the local Sherwood number $Sh_{x^*}/Ra_{x^*}^{\frac{1}{2}n}$ for two values of exponent of VWT/VWC λ ($\lambda = 0, 1$) and the power-law index n (n = 0.5, 2.0), respectively. For the fixed n, it is shown that the local Nusselt number increases as the exponent of VWT/VWC λ increases. This is because that the increase in the value of the exponent of VWT/VWC λ implies the increase of the buoyancy force which tends to accelerate the flow and raises both the dimensionless wall temperature gradient and the dimensionless wall concentration gradient (Figs. 6 and 7), and thus enhances both the local Nusselt number and the local Sherwood number, which could be also confirmed with the help of equations (27)-(28).

For the fixed λ , not only the local Nusselt number but also the local Sherwood number decreases as the power-law index n is increased. Increasing the power-law index tends to retard the velocity of the flow, thus lowering the local Nusselt

number as well as the local Sherwood number. Thus pseudoplastic fluids (n=0.5) are superior to the dilatant fluids (n=2.0) from the viewpoint of the heat and mass transfer rates by natural convection from a vertical truncated cone embedded in a porous medium saturated with power-law fluids.

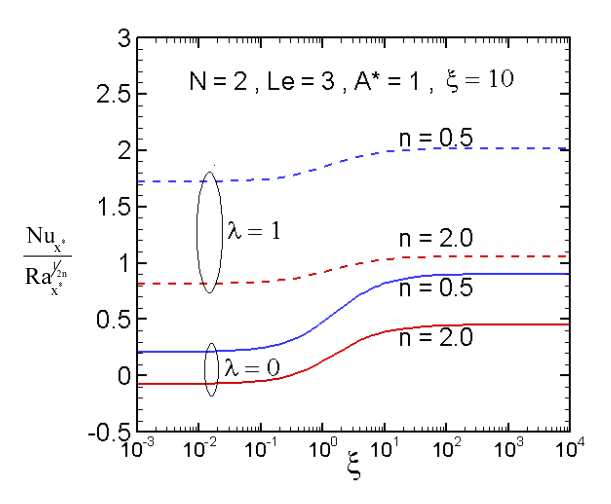


Fig. 12. Effect of n and λ on the local Nusselt number

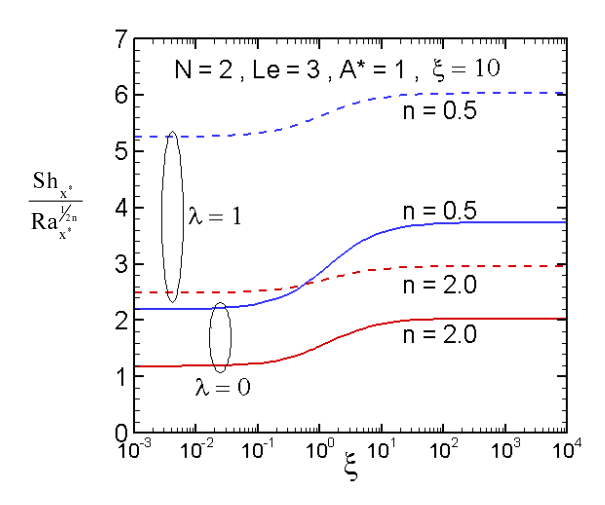


Fig. 13. Effect of n and λ on the local Sherwood number

For the purpose of the comparison with the future study, Tables 6 and 7 show the values of

 $Nu_{x^*}/Ra_{x^*}^{\frac{1}{2n}}$ and $Sh_{x^*}/Ra_{x^*}^{\frac{1}{2n}}$ for the various representative values of A^* , n, λ , and ξ with N=4, Le=10, respectively. Generally speaking, it is found that increasing the exponent of VWT/VWC λ and the dimensionless streamwise coordinate ξ enhances the local Nusselt number as well as the local Sherwood number. The local Nusselt (Sherwood) number decreases (increases) as the internal heat generation coefficient A^* . An increase in the power-law index n of fluids tends to reduce both the local Nusselt number and the local Sherwood number.

Table 6 The values of $Nu_{x^*}/Ra_{x^*}^{\frac{1}{2^n}}$ for various values of A^* , n, λ , and ξ with N=4, Le=10

A*	n	λ	$Nu_{x^*} / Ra_{x^*}^{\frac{1}{2}n}$		
A	11	,,	$\xi = 0$	$\xi = 1$	$\xi \to \infty$
0	0.5	0.0	1.0105	1.3229	1.7511
		0.5	1.9584	2.1580	2.4108
	1.0	0.0	0.6811	0.8914	1.1797
			(0.6810)		(1.1795)
		0.5	1.2206	1.3603	1.5434
			(1.2205)		(1.5431)
	2.0	0.0	0.6030	0.7892	1.0443
		0.5	1.0203	1.1501	1.3208
1	0.5	0.0	0.2404	0.5371	0.9984
		0.5	1.2846	1.4602	1.7081
	1.0	0.0	-0.0191	0.1995	0.5429
		0.5	0.6468	0.7777	0.9714
	2.0	0.0	-0.0837	0.1224	0.4437
		0.5	0.4604	0.5912	0.7839

Results in parentheses are those of Yih [31]

Table 7 The values of $Sh_{x^*}/Ra_{x^*}^{\frac{1}{2}n}$ for various values of A^* , n, λ , and ξ with N=4, Le=10

	A^*	n	λ	S	$\operatorname{Sh}_{\mathbf{x}^*}/\operatorname{Ra}_{\mathbf{x}^*}^{\frac{1}{2}r}$	1
	11			$\xi = 0$	$\xi = 1$	$\xi \to \infty$
	0	0.5	0.0	6.3671	8.3276	11.0144
ĺ			0.5	11.9022	13.2423	14.8564
Ī		1.0	0.0	3.2892	4.3043	5.6954

			(3.2897)		(5.6977)
		0.5	5.6856	6.4114	7.3168
		0.5	(5.6873)		(7.3210)
	2.0	0.0	2.4022	3.1438	4.1600
		0.5	3.9682	4.5098	5.2009
1	0.5	0.0	6.4412	8.4002	11.0893
		0.5	11.9786	13.3193	14.9330
	1.0	0.0	3.3311	4.3454	5.7367
		0.5	5.7266	6.4527	7.3573
	2.0	0.0	2.4247	3.1659	4.1820
		0.5	3.9901	4.5318	5.2222

Results in parentheses are those of Yih [31]

5. Conclusions

A two-dimensional laminar boundary layer analysis is presented to study the effect of the internal heat generation on the natural convection flow of non-Newtonian power-law fluids in a Darcy porous medium resulting from combined heat and mass buoyancy effects adjacent to the vertical truncated cone maintained at variable wall temperature and variable wall concentration (VWT/VWC). The internal heat generation is of an exponential decaying form. The transformed nonsimilar governing equations are obtained, with the coordinate transformation being performed, and then solved by Keller box method (KBM). Comparisons with previously published work are performed and excellent agreement is obtained. Numerical solutions are obtained for different values of the internal heat generation coefficient A*, the power-law index n, the dimensionless streamwise coordinate ξ , the exponent of VWT/VWC λ , the buoyancy ratio N, and the Lewis number Le. The decay of the dimensionless temperature and concentration profiles has been almost observed except for the some special cases, for example: N = -0.5. It is shown that for the increase in the value of exponent of VWT/VWC λ , the buoyancy ratio N, and the dimensionless streamwise coordinate ξ , both the local Nusselt number and the local Sherwood number increase. The local Nusselt number decreases as the internal heat generation coefficient A* and the Lewis number Le are increased. Contrary, the local Sherwood number increases with A* and Le are increased. It is also observed that the Lewis number Le has a pronounced effect on the local mass transfer rate than it does on the local heat transfer rate. A decrease in the power-law index n of fluids tends to increase the local Nusselt number as well as the local Sherwood number from a vertical truncated cone in a porous medium saturated with non-Newtonian power-law fluids. In addition, both the local Nusselt number and the local Sherwood number approach to the limits of the vertical flat plate as $\xi = \gamma = 0$ and the vertical full cone as ξ is very large ($\xi = 10^4$).

Nomenclature

Nomencla	ture
A^*	internal heat generation coefficient
a	positive constant
b	positive constant
C	concentration
D_{M}	mass diffusivity
f	dimensionless stream function
g	gravitational acceleration
h_{x^*}	local convective heat transfer coefficient
h_{m,x^*}	local convective mass transfer coefficient
K(n)	permeability of the porous medium
k	equivalent thermal conductivity
Le	Lewis number
$m_{\rm w}$	local mass flux
N	buoyancy ratio
n	power-law index of the non-Newtonian fluid
Nu_{x^*}	local Nusselt number
p	pressure

local heat flux $q_{\rm w}$ Ra_v* modified local Rayleigh number local radius of the truncated cone Sh_v* local Sherwood number Т temperature Darcy velocity in the x-direction Darcy velocity in the y-direction streamwise coordinate Х \mathbf{x}^* distance measured from the leading edge of the truncated cone distance of the leading edge of truncated X_o cone measured from the origin transverse coordinate У

Greek symbols

equivalent thermal diffusivity α coefficient of concentration expansion $\beta_{\rm C}$ coefficient of thermal expansion β_{T} half angle of the truncated cone γ pseudo-similarity variable η θ dimensionless temperature exponent of VWT/VWC λ modified viscosity μ dimensionless streamwise coordinate density dimensionless concentration stream function

Subscripts

w condition at the wall∞ ambient

References

- Nield, D. A., and Bejan, A., Convection in Porous Media, 4th edn. Springer, New York, 2013.
- 2. D. B. Ingham and I. Pop, Transport Phenomena

- in Porous Media III, Elsevier, Oxford, 2005.
- 3. Vafai, K., Handbook of Porous Media, 2nd edn. Mercel Dekker, New York, 2005.
- 4. Chen, H. T., and Chen, C. K., "Free convection of non-Newtonian fluids along a vertical plate embedded in a porous medium," J. Heat Transfer, Vol. 110, pp. 257-260 (1988).
- 5. Wang, C. Y., and Tu, C. J., "Boundary-layer flow and heat transfer of non-Newtonian fluids in porous media," Int. J. Heat Fluid Flow, Vol. 10, pp. 160-165 (1989).
- Gorla, R. S. R., and Kumari, M., "Nonsimilar solutions for free convection in non-Newtonian fluids along a vertical plate in a porous medium," Int. J. Num. Methods Heat Fluid Flow, Vol. 9, pp. 847-859 (1999).
- 7. Nakayama, A., and Koyama, H., "Buoyancy-induced flow of non-Newtonian fluids over a non-isothermal body of arbitrary shape in a fluid-saturated porous medium," Appl. Sci. Res., Vol. 48, pp. 55-70 (1991).
- Hossain, M. A., and Nakayama, A., "Nonsimilar free convection boundary layer in non-Newtonian fluid-saturated porous media," J. Thermophys. Heat Transfer, Vol. 8, pp. 107-112 (1994).
- 9. Yang, Y. T., and Wang, S. J., "Free convection heat transfer of non-Newtonian fluids over axisymmetric and two-dimensional bodies of arbitrary shape embedded in a fluid-saturated porous medium," Int. J. Heat Mass Transfer, Vol. 39, pp. 203-210 (1996).
- Wang, S. C., Chen, C. H., and Yang, Y. T.,
 "Natural convection of non-Newtonian fluids through permeable axisymmetric and two-dimensional bodies in a porous medium," Int. J. Heat Mass Transfer, Vol. 45, pp. 393-408

(2002).

- 11. Yih, K. A., "Uniform lateral mass flux effect on natural convection of non-Newtonian fluids over a cone in porous media," Int. Commun. Heat Mass Transfer, Vol. 25, pp. 959-968 (1998).
- 12. Cheng, C. Y., "Natural convection heat transfer of non-Newtonian fluids in porous media from a vertical cone under mixed thermal boundary conditions," Int. Commun. Heat Mass Transfer Vol. 36, pp. 693-697 (2009).
- 13. Mahmoud, M. A. A., "Radiation effect on free convection of a non-Newtonian fluid over a vertical cone embedded in a porous medium with heat generation," J. Appl. Mech. Tech. Phys., Vol. 53, pp. 743-750 (2012).
- 14. Rastogi, S. K., and Poulikakos, D., "Double-diffusion from a vertical surface in a porous region saturated with a non-Newtonian fluid," Int. J. Heat Mass Transfer, Vol. 38, pp. 935-946 (1995).
- 15. Cheng, C. Y., "Natural convection heat and mass transfer from a vertical truncated cone in a porous medium saturated with a non-Newtonian fluid with variable wall temperature and concentration," Int. Commun. Heat Mass Transfer, Vol. 36. pp. 585-589 (2009).
- 16. Cheng, C. Y., "Double diffusion from a vertical truncated cone in a non-Newtonian fluid saturated porous medium with variable heat and mass fluxes," Int. Commun. Heat Mass Transfer, Vol. 37. pp. 261-265 (2010).
- Crepeau, J. C., and Clarksean, R., "Similarity solutions of natural convection with internal heat generation," J. Heat Transfer, Vol. 119, pp. 183-185 (1997).
- 18. Postelnicu, A., and Pop, I., "Similarity solutions

- of free convection boundary layers over vertical and horizontal surfaces in porous media with internal heat generation," Int. Commun. Heat Mass Transfer, Vol. 26, pp. 1183-1191 (1999).
- 19. Postelnicu, A., Grosan, T., and Pop, I., "Free convection boundary-layer over a vertical permeable flat plate in a porous medium with internal heat generation," Int. Commun. Heat Mass Transfer, Vol. 27, pp. 729-738 (2000).
- 20. Bagai, S., "Similarity solutions of free convection boundary layers over a body of arbitrary shape in a porous medium with internal heat generation," Int. Commun. Heat Mass Transfer, Vol. 30, pp. 997-1003 (2003).
- 21. Bagai, S., "Effect of variable viscosity on free convection over a nonisothermal axisymmetric body in a porous medium with internal heat generation," Acta Mech., Vol. 169, pp. 187-197 (2004).
- 22. Mohamed, E. A., "The effect of lateral mass flux on the natural convection boundary layers induced by a heated vertical plate embedded in a saturated porous medium with internal heat generation," Int. J. Thermal Sci., Vol. 46, pp. 157-163 (2007).
- 23. Grosan, T., and Pop, I., "Free convection over vertical flat plate with a variable wall temperature and internal heat generation in a porous medium saturated with a non-Newtonian fluid," Tech. Mech., Vol. 21, pp. 313-318 (2001).
- 24. Grosan, T., Postelnicu, A., and Pop, I., "Free convection boundary layer over a vertical cone in a non-Newtonian fluid saturated porous medium with internal heat generation," Tech. Mech., Vol. 24, pp. 91-104 (2004).
- 25. Bagai, S., and Nishad, C., "Free convection in a non-Newtonian fluid along a horizontal plate

- embedded in porous media with internal heat generation," Int. Commun. Heat Mass Transfer, Vol. 39, pp. 537-540 (2012).
- 26. Yih, K. A., and Huang C. J., "Effect of internal heat generation on free convection heat and mass transfer of non-Newtonian fluids flow over a vertical plate in porous media: VWT/VWC," 2014 AASRC Conference, A-13, pp. 1-8 (2014)
- 27. Hong, J. T., Yamada, Y., and Tien, C. L., "Effects of non-Darcian and non-uniform porosity on vertical plate- natural convection in porous media," J. Heat Transfer, Vol. 109, pp. 356-362 (1987).
- 28. Christopher, R. V., and Middleman, S., "Power-law flow through a packed tube," Ind. Engrg. Chem. Fund., Vol. 4, pp.424-426 (1965).
- Dharmadhirkari, R. V., and Kale, D. D., "Flow of non-Newtonian fluids through porous media," Chem. Engrg. Sci., Vol. 40, pp. 527-529 (1985).
- 30. Cebeci, T., and Bradshaw, P., Physical and Computational Aspects of Convective Heat Transfer, Springer-Verlag, New York, 1984.
- 31. Yih, K. A., "Coupled heat and mass transfer by free convection over a truncated cone in porous media: VWT/VWC or VHF/VMF," Acta Mech., Vol. 137, pp. 83-97 (1999).

航空技術學院學報 第十四卷 第一期(民國一〇四年)